


Free, partial, and fully constrained recovery analysis of cold-programmed shape memory epoxy/carbon nanotube nanocomposites: Experiments and predictions

R Abishera, R Velmurugan  and KV Nagendra Gopal

Journal of Intelligent Material Systems
and Structures
1–13
© The Author(s) 2018
Reprints and permissions:
sagepub.co.uk/journalsPermissions.nav
DOI: 10.1177/1045389X18758187
journals.sagepub.com/home/jim


Abstract

Thermally activated shape memory polymers are typically programmed by initially heating the material above the glass transition temperature (T_g), deforming to the desired shape, cooling below T_g , and unloading to fix the temporary shape. This process of deforming at high temperatures becomes a time-, labor-, and energy-expensive process while applying to large structures. Alternatively, materials with reversible plasticity shape memory property can be programmed at temperatures well below the glass transition temperature which offers several advantages over conventional programming. Here, the free, partial, and fully constrained recovery analysis of cold-programmed multi-walled carbon nanotube-reinforced epoxy nanocomposites is presented. The free recovery analysis involves heating the temporary shape above T_g without any constraints (zero stress), and for fully constrained recovery analysis, the temporary shape is held constant while heating. The partially constrained recovery behavior is studied by applying a constant stress of 10%, 25%, and 50% of the maximum recovery stress obtained from the completely constrained recovery analysis. The samples are also characterized for their thermal, morphological, and mechanical properties. A non-contact optical strain measurement method is used to measure the strains during cold-programming and shape recovery. The different recovery behaviors are analyzed by using a thermo-viscoelastic–viscoplastic model, and the predictions are compared with the experimental results.

Keywords

Carbon nanotubes, shape memory polymer, plastic deformation, stress relaxation, thermomechanical properties, prediction

Introduction

The ability to store and recover large deformations, low-cost, ease-of-processing, tailorable material properties and response to wide range of stimuli have made shape memory polymers (SMPs) as ideal candidate for a wide range of applications (Lendlein and Kelch, 2002). Thermally activated SMPs have been extensively studied for applications in small-scale devices such as actuators, sensors, and biomedical stents (Sun et al., 2012) to large-scale deployable aerospace structures (Liu et al., 2014). Typically, a temporary shape is imparted on an SMP device at temperatures higher than the glass transition temperature (T_g), cooling below T_g while holding the deformation and subsequent unloading to fix the temporary shape. Although the conventional hot-programming approach is being

used in small-scale devices, programming at high temperatures becomes a complicated task when applied to large structures. Hence, it is necessary to develop and study alternate programming techniques for application in large structures. The reversible plasticity shape memory (RPSM) property provides an alternate cold-programming approach. The RPSM programming involves the following steps; (1) deforming the material plastically to a temporary shape at a temperature well

Department of Aerospace Engineering, Indian Institute of Technology Madras, Chennai, India

Corresponding author:

R Velmurugan, Department of Aerospace Engineering, Indian Institute of Technology Madras, Chennai 600036, India.
Email: ramanv@iitm.ac.in

below T_g , (2) holding the deformation to allow stress relaxation, and (3) unloading to fix the temporary shape. Finally, the material is heated above T_g to recover the original shape, thus completing the shape memory thermomechanical cycle. This simplified programming step offers several advantages over the conventional programming process such as higher recovery ratio, faster recovery rate, and improved recovery stress (Lakhera et al., 2012; Xie, 2011; Zhang et al., 2016). It is to be noted that RPSM effect can be realized only when the material is deformed above the elastic limit (yield point) where there is plastic deformation and within a limit where no permanent defects (such as cracks) occur. Also by cold-programming, 100% shape fixity cannot be obtained due to the instantaneous recovery of elastic deformation.

The effect of deformation temperature (T_d) on the shape memory behavior was studied by Yakacki et al. (2008) and Gall et al. (2005). They showed that the failure strain is maximum when T_d is at the onset of the glass transition rather than above T_g . Studies by Feldkamp and Rousseau (2010) on an epoxy-based SMP showed that the failure strain increased by five times at the onset of T_g . The above studies indicate that the onset of the glass transition must be just above the room temperature to realize RPSM effect at large plastic strains. Li and Xu (2011) studied the effect of stress relaxation on the shape fixity under cold-compression in a polystyrene-based SMP. They showed that the shape fixity increased (>90%) with the increase in relaxation time. The cold-programming technique has also been used in designing thermally activated self-healing systems such as “shape memory–assisted self-healing (SMASH)” (Rodriguez et al., 2011), a biomimetic two-step “seal and then heal” polymeric system (Li and Uppu, 2010; Nji and Li, 2010), and systems to heal surface defects (Wornyo et al., 2007; Xiao et al., 2010).

Although SMPs have exceptional shape memory properties, their low mechanical properties and the inherent insulating properties limit their applications. Reinforcing the bulk polymer with nano-fillers has proven to be an efficient approach to overcome these drawbacks (Koo, 2006; Velmurugan and Mohan, 2004, 2009). Among these nano-fillers, carbon nanotubes (CNT) have attracted special attention due to their exceptional mechanical, thermal, and electrical properties (Thostenson et al., 2001). Previous studies (Hashmi et al., 2014, 2015; Ni et al., 2007) have successfully shown that addition of CNTs not only improves the matrix properties but also assists in retaining and/or enhancing the shape memory behavior at the same time. Recently (Abishera et al., 2016), the RPSM property of multi-walled CNT (MWCNT)–reinforced epoxy nanocomposites has been reported. The glass transition temperature of a commercially available epoxy resin was tailored to realize large plastic deformations at

room temperature, and the properties were further improved by MWCNT reinforcement. The authors also systematically investigated the RPSM behavior of the nanocomposites under various programming conditions such as strain rate, deformation level, and stress relaxation time. The results indicate an excellent shape memory behavior with a potential to be used as an alternate to conventional programming.

This article aims to study the free and constrained recovery behavior of CNT/epoxy nanocomposites programmed by cold-programming. The material is characterized for its thermal, mechanical, and morphological properties, and the results are discussed. The deformation and recovery strains are measured using an optical strain measurement (OSM) technique. The different recovery behavior is also analyzed theoretically by using a thermo-viscoelastic–viscoplastic model, and the predictions are compared with the experimental results.

Experimental methods

Material selection and fabrication

The materials used in this study are diglycidyl ether of bisphenol A (DGEBA; Araldite LY556), neopentyl glycol diglycidyl ether (NGDE), poly(propylene glycol) *bis*(2-aminopropyl) ether (Jeffamine 230), and high-purity MWCNTs. All materials are used in as-received condition.

The weight ratio of DGEBA to NGDE to Jeffamine 230 used in this study is 3:2:2. The steps involved in the sample preparation are as follows: DGEBA, NGDE, and MWCNT are mixed using a mechanical stirrer at 1500 r/min for 4 h. After mixing, Jeffamine 230 is added to the mixture and stirred at the same speed for another 15 min. The mixture is poured into a silicone mold and cured at room temperature for 18 h, de-molded, and post-cured at 80°C for 2 h. Dog-bone shaped (ASTM D638 Type IV) samples are used to characterize the shape memory behavior under tensile deformations. Samples with 0, 0.5, 1, 1.5, and 2 phr MWCNT in DGEBA–NGDE–Jeffamine 230 system are prepared. It is observed that the mechanical properties of the nanocomposites with small MWCNT content (upto 2 phr) showed qualitatively similar stress–strain curves with linearly varying mechanical properties. Several previous studies (Bai and Allaoui, 2003; Montazeri et al., 2010; Montazeri and Montazeri, 2011; Rajkumar et al., 2017) on similar composite systems have also shown that for small MWCNT content, the material properties increased linearly with the addition of nano-fillers. For this reason and also for the sake of brevity, henceforth the discussions are focused on neat epoxy (E-0-CNT) and a representative nanocomposite (E-1-CNT) with 1 phr MWCNT in the epoxy matrix. At least three samples are tested for each experiment, and the average values are presented.

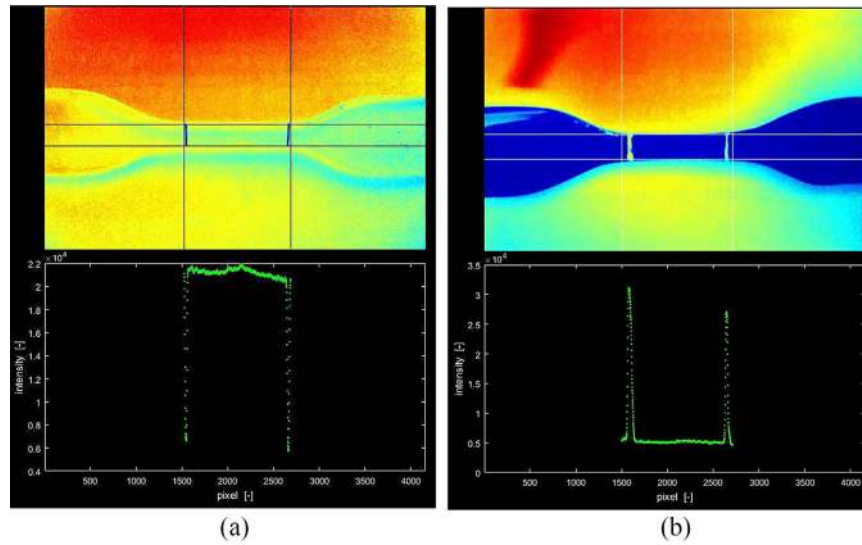


Figure 1. Screen-shots of the OSM program user interface showing the test samples and the intensity profile. The horizontal and vertical lines bound the test region: (a) neat epoxy and (b) reinforced epoxy.

Material characterization

Thermal characterization. Differential scanning calorimeter (DSC) of M/s Netzsch DSC 200 F3 Maia is used to study the glass transition properties. The DSC heating curves of all the samples are obtained for a temperature range of -30°C to 100°C in a nitrogen atmosphere. The heating rate is fixed at $10^{\circ}\text{C}/\text{min}$. A push-rod dilatometer is used to measure thermal expansion coefficient of the samples.

Morphological characterization. The morphology of the acquired MWCNTs and the fractured surfaces of different specimens is studied with the help of field emission scanning electron microscope (FESEM) of M/s FEI Quanta 3D FEG. The samples are fractured in room temperature at a strain rate of $0.0013/\text{s}$.

Mechanical characterization. A universal testing machine (UTM) fitted with an 1-kN load cell and a thermal chamber along with an OSM program is used to study and characterize the tensile performance of various samples. The engineering stress versus time data are obtained from the UTM, and the engineering strain versus time data are obtained from the OSM program. The samples are tested at room temperature (27°C), 55°C , and 80°C at a strain rate of $0.0013/\text{s}$.

OSM

The OSM technique used in this study involves a camera and an OSM MATLAB program by Frank and Spolenak (2008). The camera is used to capture the tensile deformation, and the video is converted into images. The program is able to measure the length in

pixels between two marks on the specimen. As shown in Figure 1, the marks are in high contrast to the specimen and represent the gage length. The strain is measured as the distance between these two high-contrast marks varies. The advantages of OSM include non-contact strain measurement and facilitates strain measurement in cases where testing is conducted in a temperature-controlled environment, and where attaching a strain measuring device is inconvenient or may damage the sample. Also, this method is significantly cost-effective when compared to other methods such as digital image correlation, large-scale extensometer, and laser extensometer (Liljenhjerde et al., 2016; Raasch et al., 2015).

To validate the methodology, two high-contrast strips are fixed in each of the tensile grips and the cross-head is moved at a constant speed. The translatory motion of the moving strip recorded by the cross-head and the OSM program is compared, and the results are shown in Figure 2. It is observed that the OSM program is able to capture the displacement with great accuracy.

RPSM characterization

The following steps are used to obtain the RPSM properties under stress-free conditions: (1) the sample is deformed at room temperature ($T_d = 27^{\circ}\text{C}$) to a strain of 30% ($\varepsilon_d = 0.3$) at a constant strain rate ($\dot{\varepsilon}$) of $0.0013/\text{s}$, (2) the deformation is held at ε_d for a period of $\Delta t = 30$ min to allow stress relaxation in the sample, (3) the sample is instantaneously unloaded and the fixed strain (ε_f) is measured, and finally, (4) the sample is heated to a temperature $T_r = 80^{\circ}\text{C}$ at a heating rate of $\dot{T} = 3^{\circ}\text{C}/\text{min}$ under stress-free conditions to

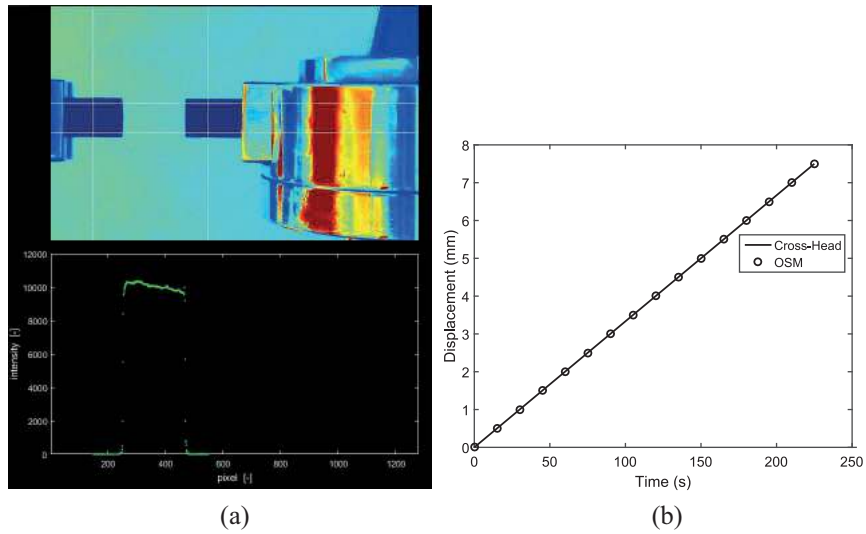


Figure 2. OSM validation: (a) screen-shot of the OSM program user interface showing high-contrast strips and intensity profile and (b) comparison between the displacement measured by the cross-head and OSM program.

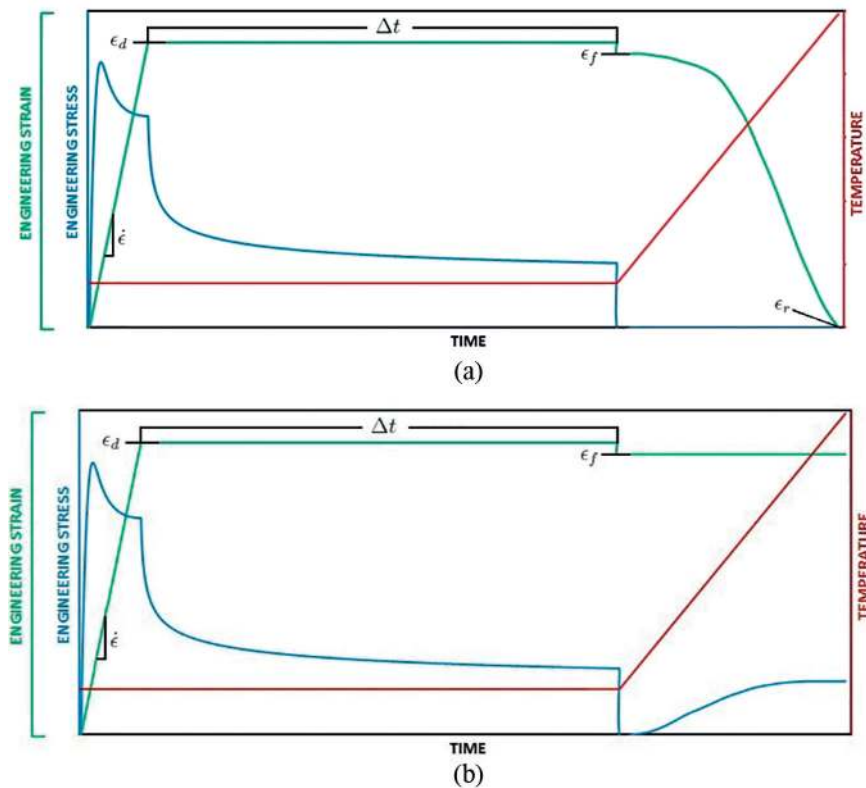


Figure 3. Temperature–stress–strain history of a typical RPSM thermomechanical cycle: (a) free recovery thermomechanical cycle and (b) constrained recovery thermomechanical cycle.

study the strain recovery of the sample. To measure the shape recovery, the sample is fixed at one end and the strain is measured using the OSM. The temperature–strain–stress history of a typical RPSM cycle is given in Figure 3. The shape fixity (R_f) and the shape recovery (R_r) are evaluated using the below equations

$$R_f = \frac{\epsilon_f}{\epsilon_d} \times 100\% \quad \text{and} \quad R_r = \frac{(\epsilon_f - \epsilon_r)}{\epsilon_f} \times 100\% \quad (1)$$

where ϵ_r is the residual strain after free recovery at T_r .

For fully constrained recovery experiments, the procedure to fix the temporary shape, that is, the programming module (Steps 1–3), is similar to that of free

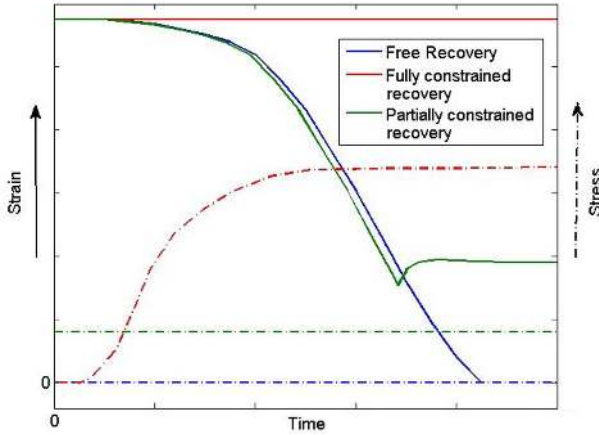


Figure 4. Schematic representation of the stress–strain history under various recovery conditions.

recovery analysis. The recovery module (Step 4) involves holding the temporary shape (i.e. keeping ε_f constant) while heating the sample above the glass transition temperature at a constant heating rate of $\dot{T} = 3^\circ\text{C}/\text{min}$. The sample is held between two grips of the UTM fitted with a thermal chamber. The force exerted by the sample during heating is measured using a high-resolution 1-kN load cell.

The recovery module for partially constrained recovery experiments involved application of a constant stress corresponding to a fraction of the recovery stress (σ_R) at 50°C obtained from the fully constrained recovery experiments. The samples are tested for partially constrained stress values of $0.1\sigma_R$, $0.2\sigma_R$, and $0.5\sigma_R$. The partially constrained temporary shape is heated above the glass transition temperature at a heating rate of $\dot{T} = 3^\circ\text{C}/\text{min}$, and the strain recovered is monitored as a function of time. A schematic of the stress–strain history under various recovery conditions is presented in Figure 4.

Model description

The principle behind the steps in an RPSM cycle can be explained as follows (Li and Xu, 2011): when the material is deformed at glassy state beyond the elastic region, the molecular segments are reorganized which in turn change its configurational entropy (Step 1). Below T_g , the plastic deformation is a rate-dependent process, so the relaxation time allows some reorientation of the deformed molecular structure wherein the stress reduces asymptotically to a non-zero value (Step 2). When the load is removed, a relaxed stress-free configuration is obtained with some elastic recovery. The plastic deformation is fixed due to the high material viscosity and reduced segmental mobility in the glassy state (Step 3).

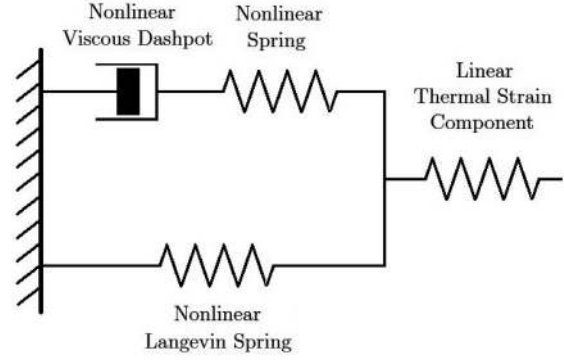


Figure 5. One-dimensional rheological analogy of the thermo-viscoelastic–viscoplastic model.

When the sample is heated above T_g , the segmental mobility increases and the material recovers back to its original configuration driven by the entropic elasticity of the rubbery state (Step 4).

Here, the one-dimensional constitutive model based on Nguyen et al. (2008) model is presented briefly to analyze the RPSM behavior under uniaxial tension. The one-dimensional rheological representation of the model is shown in Figure 5. The constitutive equations relate the following quantities:

σ	Cauchy stress
$U > 0$	Total stretch
U_T	Thermal component of the stretch
$U_M = UU_T^{-1}$	Mechanical component of the stretch
U_p	Plastic stretch
$U_e = U_M U_p^{-1}$	Elastic stretch
$\varepsilon_e = \ln U_e$	Logarithmic elastic strain
T	Temperature
T_f	Fictive temperature—structural relaxation–based internal variable
s	Strength internal variable

The constitutive equations are as follows:

1. Structural relaxation

The evolution equation for the fictive temperature (T_f) is given by

$$\frac{dT_f}{dt} = -\frac{1}{\tau_s}(T_f - T) \quad (2)$$

where τ_s is the structural relaxation time which is defined in terms of Williams–Landel–Ferry (WLF) constants (C_1, C_2) and can be expressed as follows

$$\tau_s = \tau_s^0 \exp \left[-C_1 \cdot \frac{C_2(T - T_f) + T(T_f - T_g)}{T(C_2 + T_f - T_g)} \right] \quad (3)$$

with T_g being the glass transition temperature and τ_s^o is a pre-exponential constant. Equation (2) can be generalized to include a spectrum of relaxation times, τ_{s_i}

$$\frac{dT_i}{dt} = -\frac{1}{\tau_{s_i}}(T_i - T), \quad 1 \geq i \geq q \quad (4)$$

This set of q differential equations together with the initial conditions govern the time and temperature dependence of the system when subjected to any arbitrary thermal history. Only one ($q = 1$) differential equation along with one relaxation time is considered here for simplicity. The T_g is obtained experimentally from DSC heating curves. C_1 , C_2 , and τ_s^o are obtained from curve fitting equation (5) to the DSC curves (Abishera et al., 2017)

$$P = \Delta C_p \frac{dT_f}{dt} + C_{pg} \frac{dT}{dt} \quad (5)$$

where P is the heat flow, C_{pg} and C_{pr} are the heat capacities of glassy and rubbery states, respectively, and $\Delta C_p = C_{pr} - C_{pg}$. The C_p at the onset and end of the transition region are taken as C_{pg} and C_{pr} , respectively.

2. Thermal deformation

Under the assumption that the thermomechanical response is isotropic, the thermal stretch can be written as

$$U_T = 1 + \alpha_r(T_f - T_o) + \alpha_g(T - T_f) \quad (6)$$

where α_r and α_g are the linear coefficients of thermal expansion (LCTEs) above and below T_g , respectively. The LCTEs are obtained from dilatometer experiments.

3. Equations for stress

The Cauchy stress can be additively decomposed as follows

$$\sigma = \sigma_n + \sigma_{vp} \quad (7)$$

where σ_n represents the time-independent rubbery behavior above T_g which is represented by the eight-chain network model of Arruda and Boyce (1993) and can be written as (Anand and Ames, 2006)

$$\sigma_n = \mu_r \frac{\lambda_L}{\lambda_{chain}} \mathcal{L}^{-1} \left(\frac{\lambda_{chain}}{\lambda_L} \right) [U^2 - U^{-1}] \quad (8)$$

Here, μ_r represents the rubbery state modulus and λ_L is the locking stretch. With

$$\lambda_{chain} = \sqrt{\frac{U^2 - 2U^{-1}}{3}} \quad (9)$$

and

$$\mathcal{L}(\beta) = \coth(\beta) - \frac{1}{\beta} \quad (10)$$

And σ_{vp} represents the time-dependent viscoplastic behavior of the amorphous glassy polymer below T_g and is represented as

$$\sigma_{vp} = E \varepsilon_e \quad (11)$$

where E is the initial glassy state Young's modulus. The modulus values at glassy and rubbery state are obtained from tensile tests at 27 °C and 80 °C, respectively.

4. Flow rule

The evolution equation for U_p is given as

$$\dot{U}_p = \dot{\gamma}_p U_p \quad (12)$$

Here, $\dot{\gamma}_p$ is the effective tensile plastic stretch rate and can be given in terms of T and T_f as follows

$$\dot{\gamma}_p = \frac{s}{\eta_g} \frac{T}{Q} \exp \left[C_1 \cdot \frac{C_2(T - T_f) + T(T_f - T_g)}{T(C_2 + T_f - T_g)} \right] \left\{ \sinh \left(\frac{Q}{T} \frac{\sigma_{vp}}{s} \right) - 1 \right\} \quad (13)$$

where η_g is the shear viscosity at T_g and Q is an activation parameter. s is an internal variable which represents the athermal yield strength which evolves according to the phenomenological model given by Boyce et al. (1989) as follows

$$\dot{s} = h \left(1 - \frac{s}{s_s} \right) \dot{\gamma}_p, \quad s(t = 0) = s_o, \quad s_s < s_o \quad (14)$$

where h is the flow softening modulus and s_s is the saturation value of the shear strength. The initial strength (s_o) is obtained from tensile tests at glassy state (27 °C). The parameters η_g , Q , h , and s_s are obtained by curve fitting the predictions to the uniaxial tensile and relaxation tests for different strain rates and temperatures by minimizing the error function, which is defined through

$$\Phi = 100 \sqrt{\frac{1}{N} \sum_{i=1}^N \left(1 - \frac{\sigma_{pre}^{(i)}}{\sigma_{exp}^{(i)}} \right)^2} \quad (15)$$

where N is the total number of experimental data points, $\sigma_{pre}^{(i)}$ represents the predicted stress corresponding to the i th data point, and $\sigma_{exp}^{(i)}$ represents the corresponding experimental value.

Table 1 provides the model parameters used in this study. Since the nanocomposites contain a low volume fraction (<1%) of MWCNTs and also to maintain computational simplicity, the nanocomposites are treated as a single-phase continuum at a macroscopic level, with the model parameters representing the effective properties (Yang et al., 2006). The material properties of the neat and reinforced epoxy are determined from basic micro-mechanics models and standard thermomechanical experiments. The effect of MWCNT on

Table 1. Material parameters used in the preliminary constitutive model.

Model parameter (parameter determination)	E-0-CNT	E-1-CNT (effective properties)
Glass transition temperature, T_g (DSC)	42.1 °C	44.1 °C
Programming temperature, T_o	27 °C	27 °C
Linear CTE of below T_g , α_g (dilatometer)	$0.6 \times 10^{-4} / ^\circ\text{C}$	$0.6 \times 10^{-4} / ^\circ\text{C}$
Linear CTE of above T_g , α_r (dilatometer)	$1.8 \times 10^{-4} / ^\circ\text{C}$	$1.8 \times 10^{-4} / ^\circ\text{C}$
Glassy state Young's modulus, E (tensile test at 27 °C)	450.2 MPa	616.2 MPa
Rubbery state Young's modulus, μ_r (tensile test at 80 °C)	6.5 MPa	12.8 MPa
Locking stretch, λ_L (curve fitting)	0.67	0.71
Shear viscosity at T_g , η_g (curve fitting stress–strain curves)	10,123 MPa s	24,000 MPa s
Initial shear strength, s_o (tensile test at 27)	16.77 MPa	25.77 MPa
Saturation value of shear strength, s_s (curve fitting stress–strain curves)	13.35 MPa	18 MPa
Flow activation parameter, Q (curve fitting stress–strain curves)	1899 K	2216.2 K
Flow softening modulus, h (curve fitting stress–strain curves)	250 MPa	300 MPa
First WLF constant, C_1 (curve fitting DSC curves)	33.9	35
Second WLF constant, C_2 (curve fitting DSC curves)	76.1 °C	150 °C
Structural relaxation time at T_g , τ_s^o (curve fitting DSC curves)	96.3 s	90 s

DSC: differential scanning calorimeter; CTE: coefficient of thermal expansion; WLF: Williams–Landel–Ferry.

the material behavior can be seen from the variations in the model parameters.

Results and discussions

Thermal properties

T_g is the temperature at which the SMP gets thermally activated, that is, reverts back to original shape and is a key parameter in designing SMP-based smart structures. Hence, it is significant to understand any variation in T_g with MWCNT content. The DSC heating curves of neat and filled epoxy are presented in Figure 6. The glass transition temperatures are obtained with the aid of NETZSCH Proteus software version 6.1.0. The high failure strain of the studied samples at room temperature can be attributed to the onset of glass transition being closer to room temperature (27 °C). A characteristic feature of the glass transition is an increase in polymer chain mobility in the rubbery state. Addition of MWCNT gradually increases the glass transition temperature. This effect can be attributed to the decrease in mobility of the polymer chains with the addition of MWCNTs. Addition of MWCNT had negligible effect on the LCTE values obtained from the push-rod dilatometer. Hence, the LCTE is taken as constant for both neat and filled epoxy. The measured values for LCTE are $6.04 \times 10^{-5} / ^\circ\text{C}$ and $18.92 \times 10^{-5} / ^\circ\text{C}$ for temperatures below and above T_g , respectively.

Morphological properties

FESEM micro-graphs of pristine MWCNTs and fractured surface of unreinforced and reinforced epoxy are shown in Figure 7. The MWCNTs are found to be highly pure (>95% according to the supplier) with an average length of 7.5 μm and an outer diameter of

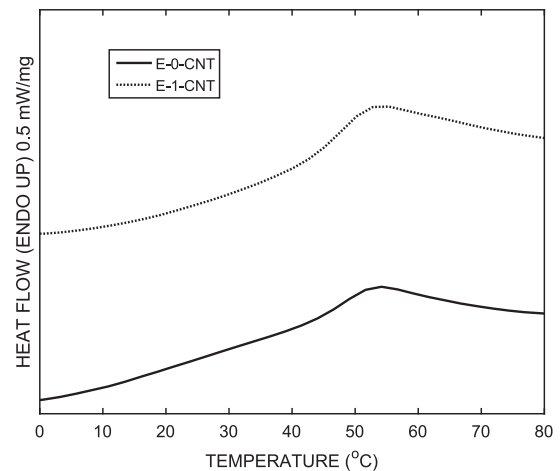


Figure 6. DSC heating curves of neat and filled epoxy.

–2040 nm yielding an average aspect ratio of 250. The fractography of neat epoxy shows a relatively smooth fracture surface indicating a ductile failure mode. At low magnifications, a considerable difference in fracture surface can be observed between neat and filled epoxy. The presence of river-bed pattern can be observed in the nanocomposites indicating a decrease in ductility. The low-magnification micro-graphs show agglomerations as bright white spots. Nevertheless, the agglomerates are uniformly distributed with an average size of less than 1 μm . The high-magnification micro-graphs show individually pulled out MWCNTs protruding from the fracture surface. It can be observed that all nanotubes including agglomerated MWCNTs are completely covered by epoxy indicating a good adhesion between MWCNT and the matrix resulting in better mechanical properties. The average effective fiber diameter of epoxy coated MWCNT is found to be 85 nm.

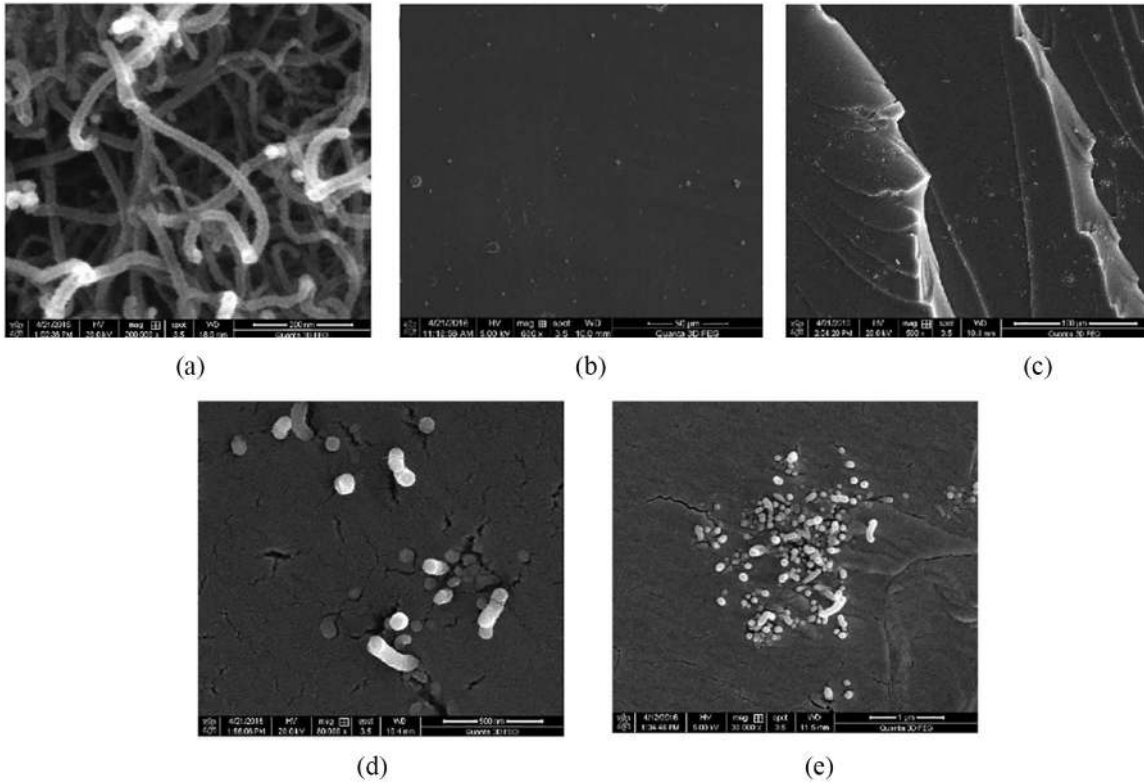


Figure 7. FESEM micro-graphs of (a) pristine MWCNT, (b) fracture surface of pure epoxy, (c) fracture surface of reinforced epoxy at low magnification ($500\times$ zoom), (d) fracture surface of reinforced epoxy at high magnification ($60,000\times$ zoom), and (e) enlarged ($35,000\times$ zoom) image of an agglomerate.

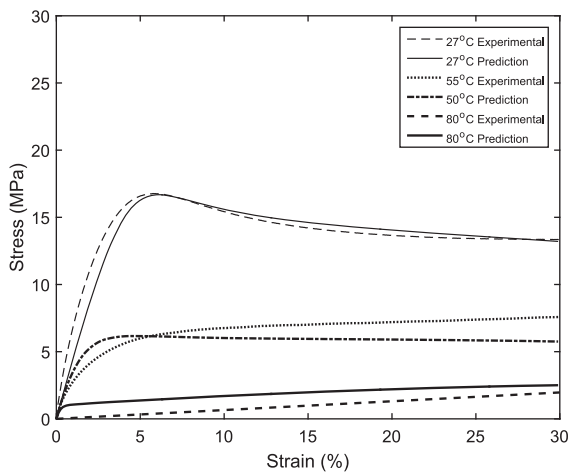


Figure 8. Effect of temperature on the tensile performance of neat epoxy.

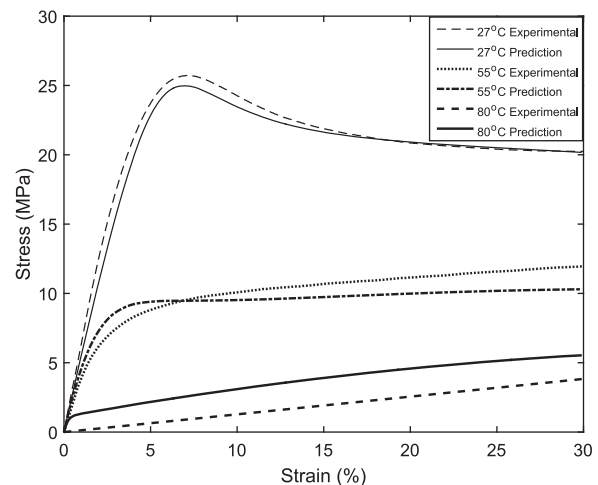


Figure 9. Effect of temperature on the tensile performance of reinforced epoxy.

Tensile properties

The experimental and predicted results of the tensile properties of neat and reinforced epoxy under different temperatures are presented in Figures 8 and 9, respectively. To avoid any relaxation effect, the samples along with the grips are heated and held at the desired

temperature for 30 min before beginning the test. The thermocouple is placed close to the samples, not on the sample so that the temperature must be considered as the temperature of air in the chamber. At room temperature (27°C), the following distinct regions can be observed: (1) an initial linear elastic region, (2) a maximum point representing the yield stress, (3) decrease in

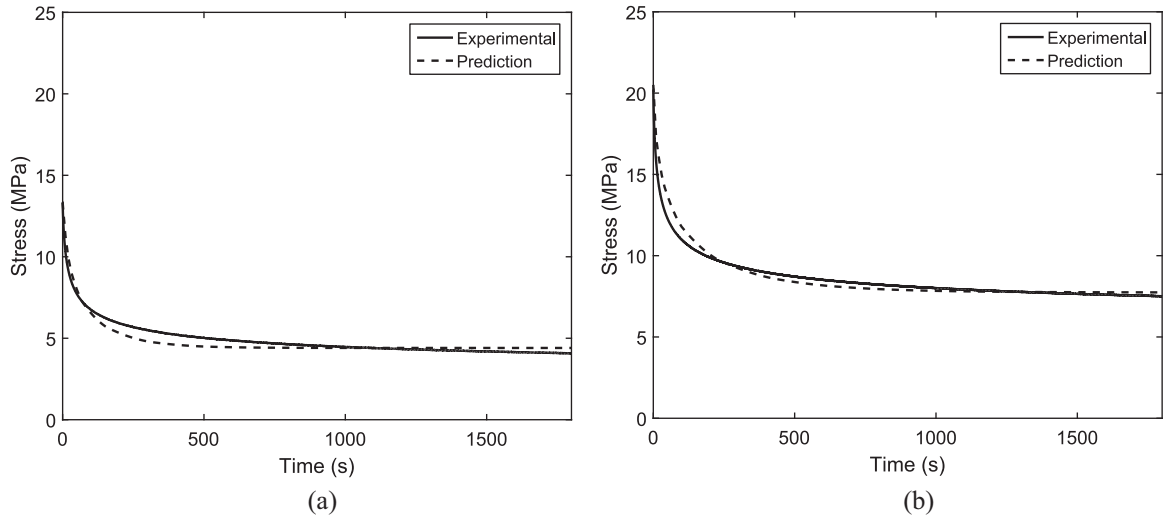


Figure 10. Stress relaxation behavior of (a) neat epoxy and (b) reinforced epoxy.

stress representing a strain softening regime, and (4) nearly constant stress region representing the plastic flow. The model is able to capture all the regions with significant accuracy.

Addition of MWCNT resulted in improved Young's modulus and yield strength indicating an effective reinforcement. The effect of temperature on the tensile performance had qualitatively similar effect on both neat and reinforced epoxy. It can be seen that an increase in temperature results in a decrease in Young's modulus and yield strength with the samples showing a rubbery behavior at temperatures well above T_g . Even at 55 °C, the samples do not show a significant yield point for the tested strain rate. The reinforcement effect of MWCNTs can also be observed at temperatures above T_g . The model is able to capture the effect of temperature on the isothermal tensile behavior of both specimens.

Stress relaxation behavior

Figure 10 presents the stress relaxation behavior of neat and reinforced epoxy. The material is deformed to a strain of 30% at a strain rate of 0.0013/s at room temperature and the deformation is held for 30 min to allow stress relaxation. Since the relaxation behavior is dependent on the viscoelastic behavior of epoxy matrix, both neat and reinforced epoxy show qualitatively similar stress relaxation behavior. It is observed that the stress reaches an asymptotic value around 20 min above which little or no stress relaxation is observed. Throughout the loading and relaxation steps, higher stress values are observed in the nanocomposites. The rate-dependent nature of the glassy state resulting in the relaxation behavior is successfully captured by the model.

The shape fixity of the cold-programmed materials significantly depends on the stress relaxation time. To

understand the effect of stress relaxation on RPSM properties, the samples are tested for four relaxation times, namely, 0, 5, 10, and 30 min, and the results are presented in Figure 11. It is observed that with a decrease in stress relaxation time, there is a significant reduction in shape fixity. For example, the shape fixity in neat epoxy after relaxation times of 0, 5, 10, and 30 min is 85.2%, 88.1%, 94%, and 96% respectively. It should be noted the shape fixity reaches a saturation value above which no amount of relaxation time will improve the shape fixity. Also, unlike conventional programming, 100% shape fixity cannot be obtained by cold drawing because a certain amount of strain is always instantaneously recovered during elastic unloading. For all relaxation times, the shape fixity in nanocomposites is higher than neat epoxy. The increase in strain fixity can be attributed to a decrease in segmental mobility with the addition of MWCNTs. Also, since stress relaxation is a characteristic of the matrix, it has qualitatively similar effect on the nanocomposites. The model is able to capture the effect of stress relaxation on the shape fixity for relaxation times of 0, 10, and 30 min and has predicted a higher shape fixity for 5 min relaxation time.

Free recovery analysis

Figure 12 presents the free recovery behavior of neat and reinforced epoxy. To study the free recovery, the sample is heated above the glass transition temperature at stress-free condition. It has been reported (Gall et al., 2005; Ping et al., 2005) that the strain recovery starts at temperatures below T_g when the programming temperature is below T_g . A similar trend is observed in this study for neat epoxy. This might be attributable to the increase in segmental mobility with an increase in temperature which would have enabled the material to

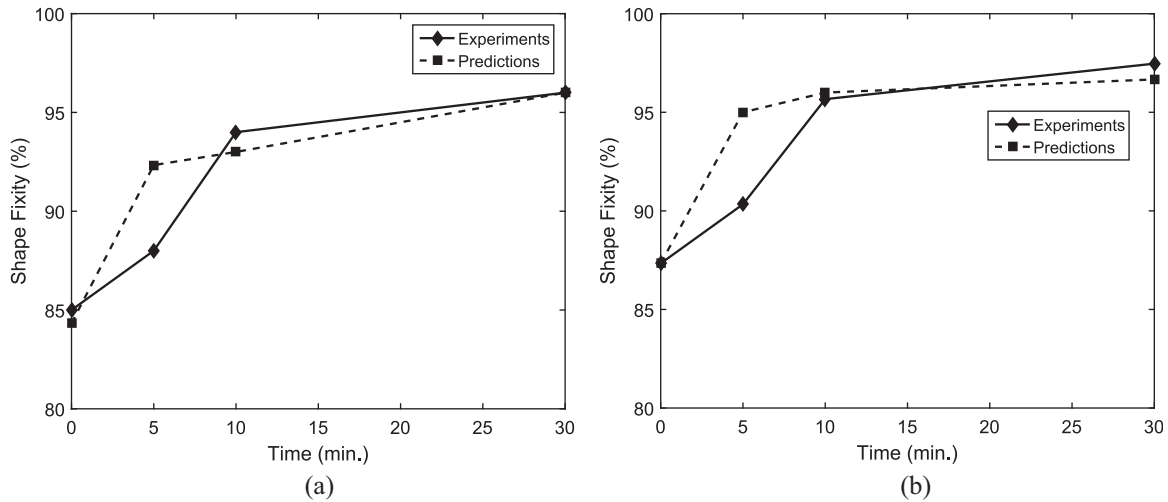


Figure 11. Effect of stress relaxation on the shape fixity: (a) neat epoxy and (b) reinforced epoxy.

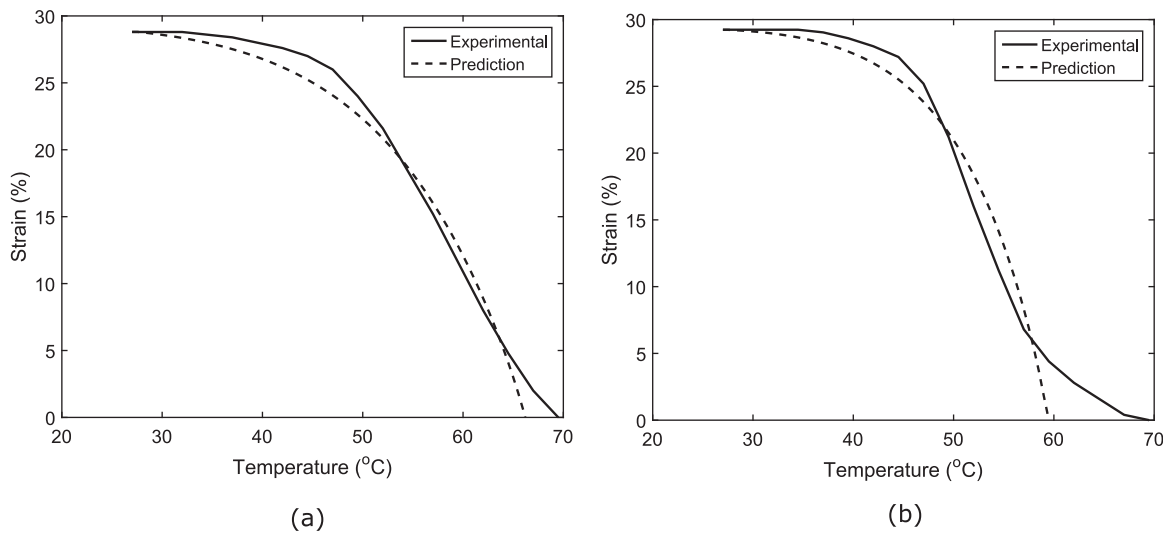


Figure 12. Free recovery analysis of (a) neat epoxy and (b) reinforced epoxy.

recover. In neat epoxy, the recovery has occurred over a range of temperature starting before the glass transition temperature and achieving a complete recovery above T_g . This is not observed in nanocomposites where the recovery begins only after the temperature has reached T_g and the stored strain is recovered completely just above T_g as shown in Figure 12. This indicates that the MWCNTs are able to successfully hold the fixed strain by restraining the segmental mobility until the temperature reaches T_g . Once the nanocomposite reaches rubbery state, the material starts to recover under entropic elasticity of the matrix, assisted by the elastic energy stored in the MWCNT resulting in a higher recovery speed. The model is able to capture the basic trend in the recovery performance of the materials. The mismatch between the experiments and predictions can be reduced by using a spectrum of structural

relaxation processes. Here, only one structural relaxation process is used for the sake of computational simplicity. Although the samples have deformed to very high strains, all samples have recovered completely when heated above T_g .

Fully constrained recovery analysis

Figure 13 presents the constrained recovery performance of neat and reinforced epoxy. After unloading and fixing the temporary shape, both ends of the sample are held between two grips of the UTM thereby keeping the strain constant. The constrained specimen is heated at a constant heating rate and the stress developed in the sample is measured using the load cell. Recovery stress defines the ability of the material to do work under thermal actuation. Stress recovery is

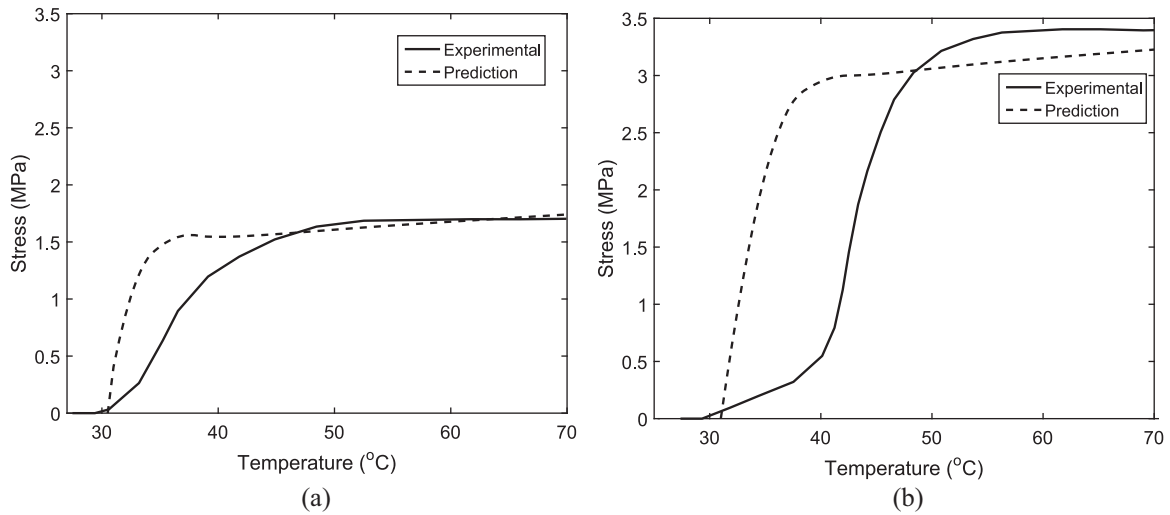


Figure 13. Constrained recovery analysis of (a) neat epoxy and (b) reinforced epoxy.

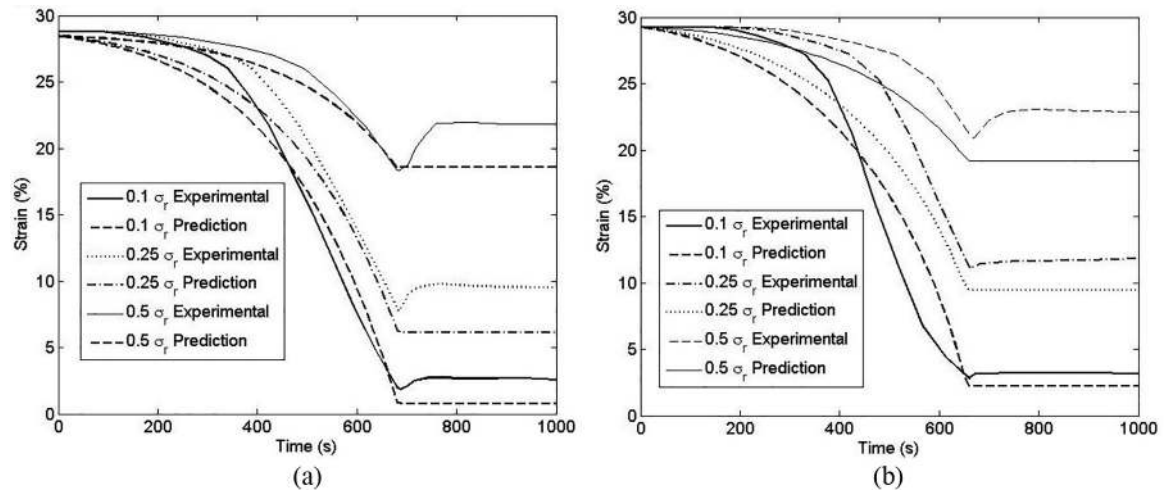


Figure 14. Experimental and predictions of partially constrained recovery analysis of (a) neat epoxy and (b) reinforced epoxy.

observed in neat epoxy at temperatures below the glass transition temperature correlating to the trend observed in the free recovery analysis. The stress reaches a maximum value just above the glass transition temperature after which the stress remains constant. The observed results are consistent with the results obtained by Li and Shojaei (2012). In reinforced epoxy, although there is gradual stress recovery below T_g , the major part of the stress recovery occurs only when the temperature reaches the glass transition temperature and rapidly reaches the maximum value. The advantage of MWCNT reinforcement can be observed in the improved recovery stress in the nanocomposites. The average maximum recovery stress (σ_r) is found to be 1.65 and 3.38 MPa for neat and reinforced epoxy, respectively (Figure 13). The model is able to capture the maximum recovery stress generated in the samples with considerable accuracy. The mismatch in the stress

recovery paths can be minimized by using multiple stress or structural relaxation process.

Partially constrained recovery analysis

Figure 14 presents the partially constrained recovery analysis of neat and reinforced epoxy. After unloading, a constant stress of 10%, 25%, and 50% of the corresponding maximum recovery stress (σ_r) is applied to the sample and heated to 70 °C at a constant heating rate. The samples are held at 70 °C for a period of 5 min to record any creep deformations. An increase in the constraining stress resulted in a decrease in the strain recovery. The average shape recovery for neat epoxy is 91.3, 67%, and 24.3%, and for reinforced epoxy it is found to be 89.7%, 59.5%, and 21.9% for 10%, 25%, and 50% σ_r , respectively. An increase in creep deformation is observed with an increase in the

constraining load. This effect is more pronounced in neat epoxy. Further increase in the constraining load has resulted in little or no shape recovery with large creep deformations when heated above T_g . It can be observed that the model was able to capture the initial strain recovery under partial constraints but was not able to capture the creep deformation at temperatures above T_g . The results can be improved by using multiple structural (equation (4)) and stress relaxation processes ($U_M^i = U_e^i U_p^i$).

Conclusion

The recovery performance of cold-programmed shape memory epoxy/CNT nanocomposites is investigated for free, partial, and completely constrained conditions. Initial mechanical characterization revealed an improvement in the Young's modulus and strength with MWCNT addition. Under free recovery conditions, all materials show excellent shape recovery behavior with 100% shape recovery. There is an improvement in the shape fixity and recovery stress with the addition of MWCNT. The effect of constraining loads on the shape recovery performance is studied. The nanocomposites showed higher recovery stress during completely constrained recovery analysis. Partially constrained recovery tests showed that with an increase in constant constraining stress, there is a decrease in shape recovery and an increase in creep deformations when heated above T_g . A thermo-viscoelastic-viscoplastic model is used to study the different recovery behavior, and the predictions are compared with the experiments. The model is able to predict the mechanical and the shape recovery behavior with significant accuracy. As a result, it is demonstrated that the cold-programming approach can be used as an alternate to conventional high-temperature programming.


Declaration of conflicting interests

The author(s) declared no potential conflicts of interest with respect to the research, authorship, and/or publication of this article.

Funding

The author(s) received no financial support for the research, authorship, and/or publication of this article.

ORCID iD

R Velmurugan  <https://orcid.org/0000-0002-8821-2926>

References

- Abishera R, Velmurugan R and Gopal KN (2016) Reversible plasticity shape memory effect in carbon nanotubes reinforced epoxy nanocomposites. *Composites Science and Technology* 137: 148–158.
- Abishera R, Velmurugan R and Gopal KN (2017) Reversible plasticity shape memory effect in epoxy/CNT nanocomposites—a theoretical study. *Composites Science and Technology* 141: 145–153.
- Anand L and Ames N (2006) On modeling the micro-indentation response of an amorphous polymer. *International Journal of Plasticity* 22(6): 1123–1170.
- Arruda EM and Boyce MC (1993) A three-dimensional constitutive model for the large stretch behavior of rubber elastic materials. *Journal of the Mechanics and Physics of Solids* 41(2): 389–412.
- Bai J and Allaoui A (2003) Effect of the length and the aggregate size of MWNTs on the improvement efficiency of the mechanical and electrical properties of nanocomposites—experimental investigation. *Composites Part A: Applied Science and Manufacturing* 34(8): 689–694.
- Boyce MC, Weber G and Parks DM (1989) On the kinematics of finite strain plasticity. *Journal of the Mechanics and Physics of Solids* 37(5): 647–665.
- Feldkamp DM and Rousseau IA (2010) Effect of the deformation temperature on the shape-memory behavior of epoxy networks. *Macromolecular Materials and Engineering* 295(8): 726–734.
- Frank S and Spolenak R (2008) *Optical Strain Measurement by Digital Image Analysis* (Matlab script). Zürich: Department of Materials, Laboratory for Nanometallurgy.
- Gall K, Yakacki CM, Liu Y, et al. (2005) Thermomechanics of the shape memory effect in polymers for biomedical applications. *Journal of Biomedical Materials Research Part A* 73(3): 339–348.
- Hashmi S, Abishera R, Chandra Prasad H, et al. (2014) Influence of air oxidized CNT reinforcement on the recovery stress of shape memory polyurethane. *International Journal of ChemTech Research* 6(3): 1873–1876.
- Hashmi S, Prasad HC, Abishera R, et al. (2015) Improved recovery stress in multi-walled-carbon-nanotubes reinforced polyurethane. *Materials & Design* 67: 492–500.
- Koo JH (2006) *Polymer Nanocomposites: Processing, Characterization, and Applications*. New York: McGraw-Hill.
- Lakhera N, Yakacki CM, Nguyen T, et al. (2012) Partially constrained recovery of (meth) acrylate shape-memory polymer networks. *Journal of Applied Polymer Science* 126(1): 72–82.
- Lendlein A and Kelch S (2002) Shape-memory polymers. *Angewandte Chemie International Edition* 41(12): 2034–2057.
- Li G and Shojaei A (2012) A viscoplastic theory of shape memory polymer fibres with application to self-healing materials. *Proceedings of the Royal Society A: Mathematical, Physical and Engineering Sciences* 468: 2319–2346.
- Li G and Uppu N (2010) Shape memory polymer based self-healing syntactic foam: 3-D confined thermomechanical characterization. *Composites Science and Technology* 70(9): 1419–1427.
- Li G and Xu W (2011) Thermomechanical behavior of thermoset shape memory polymer programmed by cold-compression: testing and constitutive modeling. *Journal of the Mechanics and Physics of Solids* 59(6): 1231–1250.
- Liljenhjerter J, Upadhyaya P and Kumar S (2016) Hyperelastic strain measurements and constitutive parameters

- identification of 3D printed soft polymers by image processing. *Additive Manufacturing* 11: 40–48.
- Liu Y, Du H, Liu L, et al. (2014) Shape memory polymers and their composites in aerospace applications: a review. *Smart Materials and Structures* 23(2): 023001.
- Montazeri A and Montazeri N (2011) Viscoelastic and mechanical properties of multi walled carbon nanotube/epoxy composites with different nanotube content. *Materials & Design* 32(4): 2301–2307.
- Montazeri A, Javadpour J, Khavandi A, et al. (2010) Mechanical properties of multi-walled carbon nanotube/epoxy composites. *Materials & Design* 31(9): 4202–4208.
- Nguyen TD, Qi HJ, Castro F, et al. (2008) A thermoviscoelastic model for amorphous shape memory polymers: incorporating structural and stress relaxation. *Journal of the Mechanics and Physics of Solids* 56(9): 2792–2814.
- Ni QQ, Zhang CS, Fu Y, et al. (2007) Shape memory effect and mechanical properties of carbon nanotube/shape memory polymer nanocomposites. *Composite Structures* 81(2): 176–184.
- Nji J and Li G (2010) A biomimic shape memory polymer based self-healing particulate composite. *Polymer* 51(25): 6021–6029.
- Ping P, Wang W, Chen X, et al. (2005) Poly (ϵ -caprolactone) polyurethane and its shape-memory property. *Biomacromolecules* 6(2): 587–592.
- Raasch J, Ivey M, Aldrich D, et al. (2015) Characterization of polyurethane shape memory polymer processed by material extrusion additive manufacturing. *Additive Manufacturing* 8: 132–141.
- Rajkumar AR, Ramachandran V, Gopal KVN, et al. (2017) Reversible plasticity shape-memory effect in epoxy nanocomposites: experiments, modeling and predictions. In: Altenbach H, Goldstein RV and Murashkin E (eds) *Mechanics for Materials and Technologies*. New York: Springer, pp. 387–415.
- Rodriguez ED, Luo X and Mather PT (2011) Linear/network poly (ϵ -caprolactone) blends exhibiting shape memory assisted self-healing (SMASH). *ACS Applied Materials & Interfaces* 3(2): 152–161.
- Sun L, Huang WM, Ding Z, et al. (2012) Stimulus-responsive shape memory materials: a review. *Materials & Design* 33: 577–640.
- Thostenson ET, Ren Z and Chou TW (2001) Advances in the science and technology of carbon nanotubes and their composites: a review. *Composites Science and Technology* 61(13): 1899–1912.
- Velmurugan R and Mohan T (2004) Room temperature processing of epoxy-clay nanocomposites. *Journal of Materials Science* 39(24): 7333–7339.
- Velmurugan R and Mohan T (2009) Epoxy-clay nanocomposites and hybrids: synthesis and characterization. *Journal of Reinforced Plastics and Composites* 28(1): 17–37.
- Wornyo E, Gall K, Yang F, et al. (2007) Nanoindentation of shape memory polymer networks. *Polymer* 48(11): 3213–3225.
- Xiao X, Xie T and Cheng YT (2010) Self-healable graphene polymer composites. *Journal of Materials Chemistry* 20(17): 3508–3514.
- Xie T (2011) Recent advances in polymer shape memory. *Polymer* 52(22): 4985–5000.
- Yakacki CM, Willis S, Luders C, et al. (2008) Deformation limits in shape-memory polymers. *Advanced Engineering Materials* 10(1–2): 112–119.
- Yang JL, Zhang Z, Schlarb AK, et al. (2006) On the characterization of tensile creep resistance of polyamide 66 nanocomposites. Part II: modeling and prediction of long-term performance. *Polymer* 47(19): 6745–6758.
- Zhang X, Tang Z and Guo B (2016) Reversible plasticity shape memory polymers: key factors and applications. *Journal of Polymer Science Part B: Polymer Physics* 54(14): 1295–1299.